AIAA JOURNAL
Vol. 47, No. 6, June 2009

Acoustic Measurements of High-Speed Jets from Rectangular Nozzle with Thrust Vectoring

Adam E. Goss,* Jérémy Veltin,† Jaehyung Lee,‡ and Dennis K. McLaughlin§
Pennsylvania State University, University Park, Pennsylvania 16802

DOI: 10.2514/1.39843

Laboratory experiments were conducted to characterize the noise produced by jets from a rectangular nozzle with thrust-vectoring capability. Such exhaust jets are present on state-of-the-art fighter aircraft designed for supermaneuverability. This scaled nozzle research was facilitated by the design of a model with rectangular exit geometry and thrust-vectoring attachments, thus simulating one configuration of such aircraft. A supersonic, helium–air mixture jet issued from this nozzle, and acoustic measurements were made with four microphones arranged in a circular arc in the far-field region. Schlieren photographs were recorded to establish the major features of the jet flow. Significant among the results was the fact that the addition of thrust-vectoring attachments set to 0 deg deflection, on an otherwise clean rectangular nozzle, decreases the intensity of sound radiated on each axis plane to below that of a round nozzle jet. Furthermore, deflection of the flow in the minor axis plane by virtue of these nozzle attachments induces an approximately corresponding deflection of the acoustic field without significant additional noise components in the peak emission direction. The frequency spectra as well as overall sound pressure levels of microphone measurements with the rectangular nozzle jet at several observation positions and thrust-vectoring configurations are presented and summarized in the results of this paper.

Nomenclature

a_a	=	ambient speed of sound
a_j	=	speed of sound at the outlet
D	=	equivalent diameter of the nozzle exit
f	=	frequency
f_C	=	characteristic frequency ($=U_j/D$)
M_d	=	nozzle design Mach number
M_j	=	Mach number of the jet
R	=	microphone physical distance to the jet outlet
St	=	Strouhal number [$=f/(U_j/D)$]
T_a	=	atmospheric temperature
T_{j0}	=	simulated jet stagnation temperature
TR	=	total temperature ratio, T_{j0}/T_a
U_j	=	jet exhaust mean velocity
β	=	a of the thrust-vectoring paddle with the nozzle axis
Δf	=	frequency bin (resolution)
θ	=	polar angle, measured from the outlet jet axis
φ	=	azimuthal angle

Introduction

RESEARCH on the noise produced by aircraft engine exhaust jets has progressed most notably in the civilian sector during the past several decades. Aside from the recently terminated High-Speed Research Program led by NASA, the focus of civilian aeroacoustic research has been on subsonic aircraft powered by high bypass ratio turbofan engines. On the military side, current high-performance supersonic U.S. Department of Defense aircraft have engines with noise characteristics that are different from their civilian counterparts. They have significantly lower bypass ratios and the majority of the thrust is generated by the core jet exhaust. The corresponding exit velocities and temperatures of the jets are extremely high and the associated noise is far greater than that of equivalent thrust high bypass ratio engines that power the civilian fleet. Military aircraft engine noise poses a health threat to ground crews (in carrier-based operations, for example), as well as causing an annoyance to communities in the vicinity of military installations. This can impact basing decisions as well as operations and training requirements. Besides this military noise reduction program, a newly emerging civilian application may reach the research forefront as the early exploratory development programs on supersonic business jets are being pursued [1].

These military and civilian developments produced the motivation for high-speed jet noise research, the most extensive of which include theoretical and experimental studies of high-speed round jets. Examples of such investigations are Tam et al. [2,3], Tanna et al. [4], Morris et al. [5], and Doty and McLaughlin [6]. The goals of the present study were to extend the Pennsylvania State University research to rectangular jets and particularly to those with thrust-vectoring nozzles. Prior experiments on noise radiated by rectangular jets performed by Seiner and Ponton [7], Massey et al. [8], and Kantola [9] showed measurable differences in the acoustic fields radiating in the major and minor axes planes. The present experiments were designed to extend and perhaps clarify the nonaxisymmetric nature of the radiated noise in comparison with former laboratory experiments using round nozzles. Additionally, the experiments would provide the initial identification of the acoustic characteristics associated with the thrust-vectoring mechanisms. Thrust vectoring is an aircraft's ability to deflect the exhaust jet to various angles for enhanced maneuverability: in the case of the class of aircraft of interest, enhanced pitch rotation. The proposed acoustic experiments would provide the initial data on the effect of thrust vectoring. A more complete and accurate study would include the flow around the aircraft (in forward flight), measurements not available in the present jet noise facility.

Experimental Facility and Procedure

Facility Description

Experiments using the rectangular nozzle were conducted in the High-Speed Jet Noise Facility at Pennsylvania State University. This facility includes a Kaeser air compressor, which pressurizes two reservoir tanks of 18.9 m^3 (6700 ft^3) each to 1.3 MPa (190 psig). The

Presented as Paper 2006-2704 at the 12th AIAA/CEAS Aeroacoustics Conference, Cambridge, MA, 8–10 May 2006; received 17 July 2008; revision received 23 January 2009; accepted for publication 5 March 2009.

*Undergraduate Student, Schreyer Honors College.
†Graduate Student, Aerospace Engineering.
‡Research Assistant, Aerospace Engineering.
§Professor of Aerospace Engineering. Fellow AIAA.

Fig. 1 Rectangular stereo lithography nozzle attached to plenum inside the anechoic chamber of the high-speed jet noise facility.

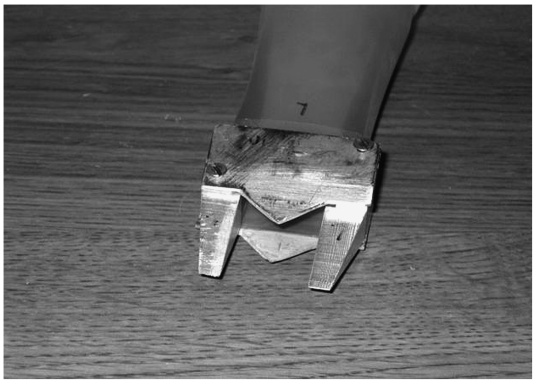

Fig. 3 Attachments for thrust-vectoring simulation (10 deg deflection angle shown).

compressed air passes through a drier and is then piped to a plenum before exhausting through a model nozzle in the facility's anechoic chamber, as pictured in Fig. 1.

For simulating hot jets, helium from three canisters pressurized at 15.9 MPa (2300 psig) is injected into the flow a sufficient distance upstream of the plenum to allow for thorough mixing with the air. Why helium effectively simulates a hot jet, as well as the implications associated with this methodology, is discussed by Doty and McLaughlin [6] and Papamoschou [10]. These references also underline the safety and economic benefits of using a helium/air mixture over actual heated air for the experiments conducted in this facility. Inside the anechoic chamber, fiberglass wedges are attached to each wall, resulting in chamber wedge-to-wedge dimensions of $5.02 \times 6.04 \times 2.79$ m ($16.5 \times 19.82 \times 9.15$ ft) and a cutoff frequency of 250 Hz. An exhaust system, beginning on the wall opposing the plenum, ingests the flow to maintain approximately constant ambient conditions inside the chamber. A schematic of this system is shown in Fig. 2 along with the various other components comprising the facility. As noted in [11], from which Fig. 2 was taken, noise from the exhaust fan is controlled primarily by two mufflers located fore and aft of the fan.

The target Mach number and simulated temperature ratio at the exit plane of the nozzle are achieved by controlling the partial pressures of both the air and helium that are mixed in the jet plenum. These (partial) pressures are measured in the settling chamber section upstream of the nozzle with a pressure transducer interfaced to the data acquisition system. The air partial pressure and mixture total pressure are the specific pressures measured just before and during an experiment. The target values for these parameters are calculated by a FORTRAN program developed by Doty and McLaughlin [6]. Inputs for this program are the Mach number and temperature ratio for the desired test case as well as the ambient temperature, pressure, and relative humidity inside the chamber. The data acquisition system is automatically triggered when it measures the transducer voltage corresponding to the correct value of plenum total pressure that will produce the desired jet Mach number and simulated temperature.

Rectangular Nozzle Design

The nozzle design started with a supersonic section designed by the method of characteristics, as described in detail by Liepmann and Roshko [12], to produce a uniform Mach 1.5 flow at the exit ($M_d = 1.5$). The subsonic portion of the nozzle is essentially a smooth conversion section from the large round inlet fitting at the outlet of the plenum to the rectangular nozzle throat. The contours of this section (and the final supersonic section) were established using the software Solid Works and produced a rectangular exit with a width-to-height aspect ratio of 1.75. This rectangular geometry has an exit area equal to a circle with an equivalent diameter of 1.76 cm (0.695 in.). Low-cost stereo lithography (SLA) was used for fabrication of the rapid prototyped model. For this paper, the azimuthal angle φ is taken to be zero on the nozzle major axis plane.

The rectangular nozzle was also designed to accommodate the attachment of thrust-vectoring paddles fabricated from two steel plate cutouts screwed onto two aluminum components designed to mate with the notch seen in the sides of the SLA nozzle in Fig. 1. The steel components were cut from 1.3 mm (1/16 in.) flat stock and the result is pictured in Fig. 3, showing the model attachments assembled on the SLA nozzle for simulation of 10 deg thrust vectoring. These

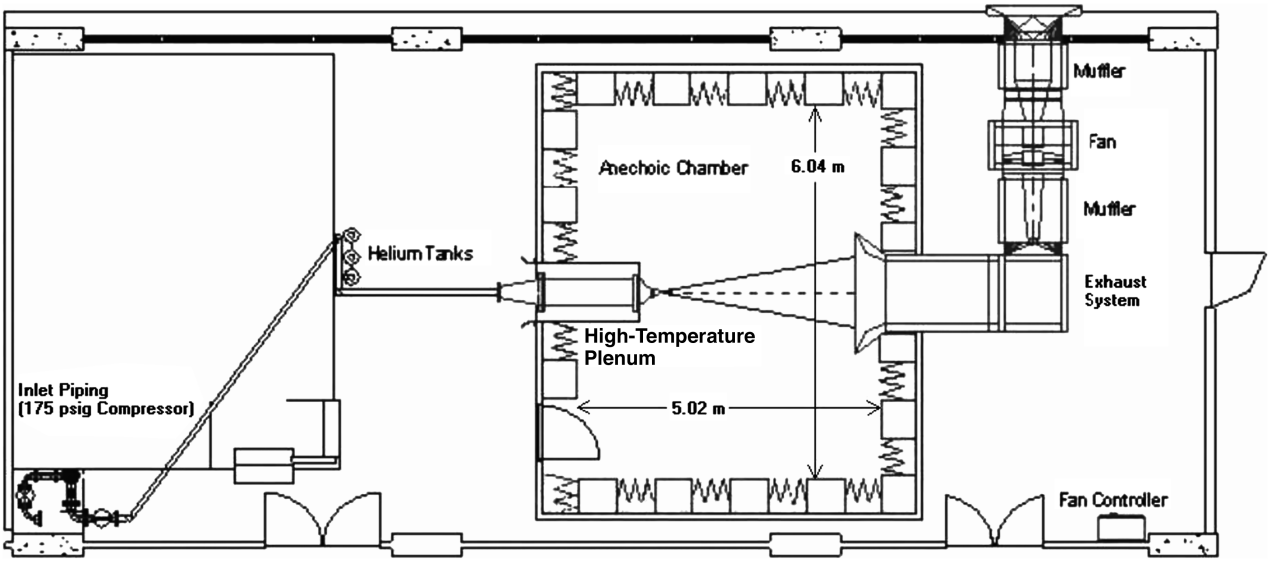

Fig. 2 Schematic of the high-speed jet noise facility at the Pennsylvania State University (Petitjean and McLaughlin [11]).

attachments serve to vector the exhaust jet at various angles in the nozzle's minor axis plane, and, for simplicity, several pairs of these plates were constructed for simulation of vectoring angles between 0 and 20 deg. Because of the immobile nature of the aluminum side attachments, only one pair of these components needed to be fabricated. When attached to the nozzle, these pieces extend from the exit plane a distance 2.5 times that of the deflection pieces when at 0 deg vectoring. Shapes and dimensions for the components were based on published information available for a modern air superiority fighter aircraft.

The present stereo lithography rapid prototype nozzle, together with the thrust-vectoring attachments, comprises the first (we are aware of) laboratory model used to measure the acoustic characteristics of such a flow. Such characteristics have a dramatic effect on the acoustic results presented in the remaining sections of this report.

Instrumentation

Four 3.2-mm-diam (1/8 in.) Brüel and Kjaer (B&K) microphones, type 4138, were used to measure the noise produced by the rectangular nozzles. Measurements were taken at four polar angles θ from the jet centerline between 0 and 90 deg at nondimensional distances $R/D = 50$ for the rectangular nozzle and $R/D = 69.5$ for the round nozzle, where R is the physical distance of the microphone from the nozzle exit plane (88 cm; 34.7 in.), and D is the diameter of an effective circular area equivalent to that of the rectangular nozzle. At approximately 25 cm (10 in.) beyond the R/D, the microphones connect to a circular boom support which is covered in fiberglass to reduce noise reflections. This support lies on a plane coincident with either the major or minor axis plane of the nozzle, depending on its orientation, or azimuth angle φ, when attached to the plenum.

The noise field is sampled automatically by the microphone array once the voltmeter (connected to the plenum's pressure transducer) reads the value corresponding to the desired test conditions. The analog time-domain signals are routed to a Nexus, B&K signal conditioner where they are amplified and passed through an anti-aliasing filter, thus enabling their exclusive digital conversion in the following acquisition. A PCI-6110 National Instruments data acquisition board acquires the time-domain data, which are then stored with the units of volts in binary files that are passed to the following stage for processing and correction. Each microphone collects 102,400 data points with a sampling rate set at 300,000 Hz.

Initial processing is carried out within the LabVIEW software and involves converting the voltage data to pressure values via multiplication by the respective microphone calibration constants. Each channel of microphone data is partitioned, and each partition is passed through a Hanning window and a fast Fourier transform. These data are averaged to yield the power spectral density (PSD) for each of the individual microphones. Further manipulation converts the PSD to a decibel scale, referenced at 20 μPa, to yield the raw sound pressure level (SPL) for each acquired signal. Raw data are then further processed to apply the necessary microphone response and atmospheric attenuation correction (the latter yields lossless acoustic data). Finally, the spectra are fully nondimensionalized to produce spectral outputs in SPL per unit Strouhal number. Equation (1) summarizes the corrections made to the raw SPL data:

$$\mathrm{SPL}(f)/\mathrm{unit}St = \mathrm{SPL}_{\mathrm{raw}}(f) - \underbrace{\Delta C_{\mathrm{act}}(f) - \Delta C_{ff}(f)}_{\text{microphone response}} + \underbrace{\Delta C_{\mathrm{atm}}(f)}_{\text{atmospheric correction}} - \underbrace{10 \cdot \log_{10}\Delta f}_{\text{scaling to1 Hz bandwidth}} + \underbrace{10 \cdot \log_{10} f_C}_{\text{Strouhal number scaling}} \quad (1)$$

The frequency is nondimensionalized by the flow's characteristic frequency defined by the jet velocity U_j divided by the jet diameter D to produce the Strouhal number as follows:

$$St = \frac{f}{U_j/D} \quad (2)$$

Further details of the microphone corrections and processing are discussed in [6,11]. To ensure that data passed to the analysis stage are free from contamination, such as noise reflections, a first look at the acquired noise spectrum is performed using LabVIEW immediately following the experiment. Any major error in the spectra, such as large amplitude oscillations indicating the presence of reflections, can often be identified before extensive processing. Based on this, measures can be taken to remove the error through correction of the setup. Following all processing, the measurements of overall sound pressure level (OASPL) and individual spectral components are estimated to have uncertainties of approximately 1 and 1.5 dB, respectively.

The acoustics instrumentation is accompanied by a conventional Z-type schlieren system that has been described in several previous publications (Holder and North [13]). Schlieren images provide important information, particularly on the deflection of the jet flow in the presence of thrust-vectoring paddles.

Acoustic Results

Measurements of the rectangular nozzle acoustic field first sought to investigate the differences between its radiated noise in comparison with data from round nozzle experiments conducted previously in the Pennsylvania State High-Speed Jet Noise Facility. Further investigation focused on the differences in the rectangular nozzle's major and minor axis planes, and also on the effect of thrust-vectoring paddles on the radiated noise. Conditions under which these initial tests were conducted are summarized in Table 1 for each nozzle type. Note that the first two rows of the table pertain to the rectangular nozzle, whereas the last row provides conditions for an axisymmetric, 12.7-mm-diam (0.5 in.) nozzle. Various comparisons among the experiments outlined in Table 1 offer initial insight into the acoustic characteristics of rectangular nozzles and the groundwork upon which thrust-vectoring results may be built. A discussion regarding this groundwork is presented in the following two subsections.

Rectangular (Major and Minor Axis Planes) vs Round Exit Geometry

Figure 4 compares fully corrected frequency spectra from measurements with the clean rectangular nozzle (no vector attachments) with those from an experiment using a 12.7-mm-diam (0.5 in.) round nozzle. The comparison is made at a jet Mach number $M_j = 1.5$ and a jet-to-ambient stagnation temperature ratio $T_{j0}/Ta = 3.6$. There are three individual spectra plotted in each part of the figure. Two are from the rectangular nozzle, showing the difference between the acoustic measurements along the major axis

Table 1 Test conditions for initial rectangular nozzle data comparisons

Nozzle	Jet Mach no., U_j/a_j	Simulated temperature, T_{j0}/T_a	Acoustic Mach no., U_j/a_a	U_j/D, kHz	Reynolds no.	Nozzle axis plane
Smooth surface (SLA)	1.5	3.6	2.37	42.48	505,000	Major, minor
0 deg vector	1.5	3.6	2.37	42.48	505,000	Major, minor
12.7 mm round	1.5	3.6	2.37	59.05	360,000	N/a

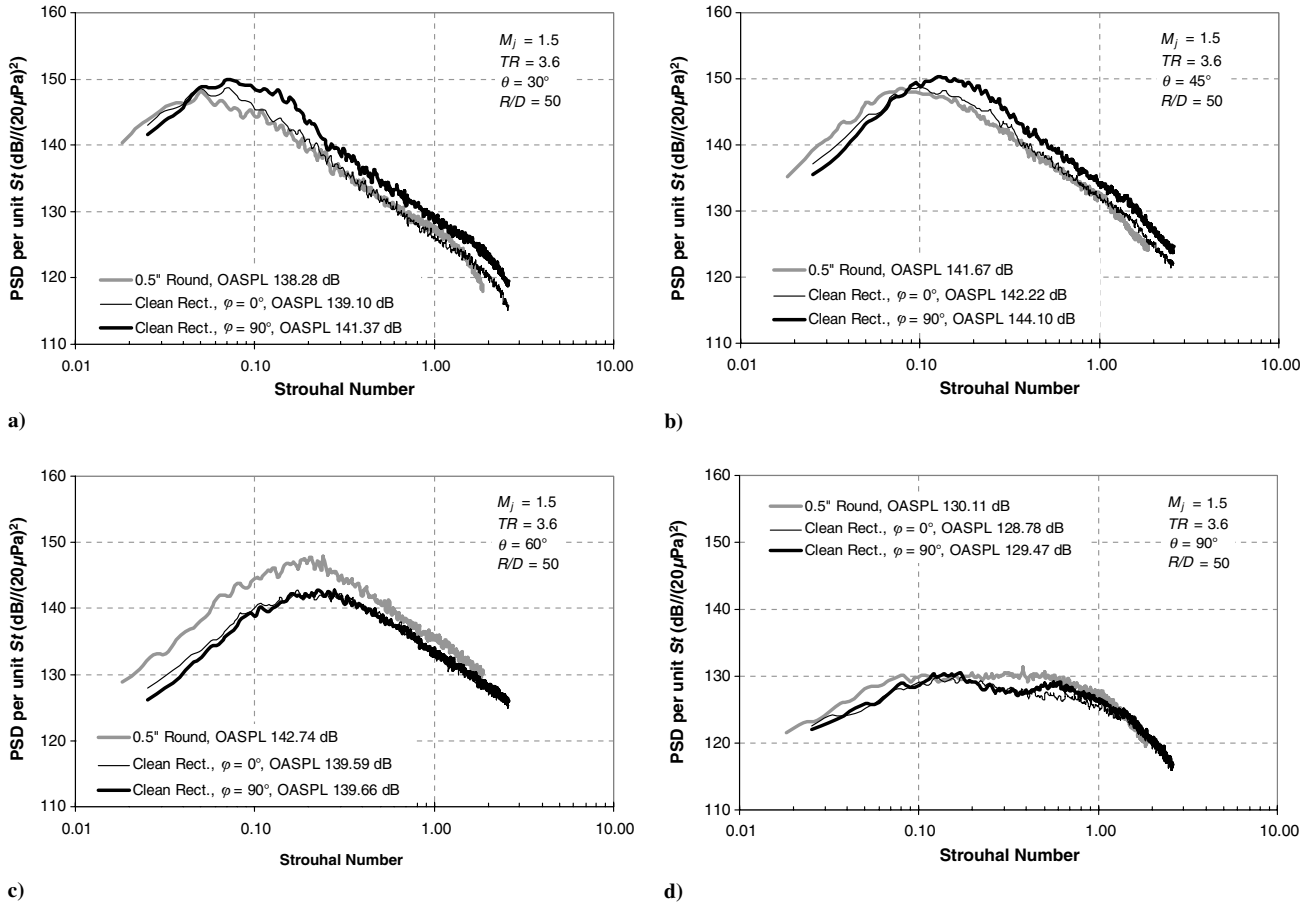

Fig. 4 Acoustic spectra for smooth rectangular nozzle ($D = 0.695$ in.) vs round nozzle ($D = 0.5$ in.): $M_j = 1.5$, $U_j/D_{\text{rect}} = 42.48$ kHz, $U_j/D_{\text{round}} = 59.05$ kHz; a) $\theta = 30$ deg, b) $\theta = 45$ deg, c) $\theta = 60$ deg, d) $\theta = 90$ deg.

plane ($\varphi = 0$ deg) and the minor axis plane ($\varphi = 90$ deg), whereas the third is from the round jet measurements. Progression from Fig. 4a to Fig. 4d shows the spectral change for each nozzle type over the observed polar angles $\theta = 30, 45, 60$, and 90 deg, measured from the jet centerline. Data for round and rectangular nozzles were both collected at a physical distance of 88 cm (34.75 in.) from the jet exit, which translates to 69.5 and 50 diameters, respectively, using each nozzle's equivalent diameter. For comparison purposes, the round jet data were scaled to 50 diameters to match the rectangular nozzle distance (assuming spherical spreading of the acoustic field).

The results show that the frequency spectra for the rectangular nozzle's major axis plane ($\varphi = 0$ deg) are comparable to those of the round geometry for polar angles 30–45 deg, whereas the minor axis plane ($\varphi = 90$ deg) is louder than the round nozzle by approximately 3 dB in the same polar range. For polar angles 60–90 deg, the spectral intensities for both rectangular planes are actually lower than the round jet case. Hence, the rectangular geometry does not provide an acoustic disadvantage in relation to round geometry, but rather an improvement for angles greater than 45 deg from the jet centerline. However, for smaller angles, the increased sound pressure levels on the minor axis plane do pose a disadvantage for the use of the rectangular geometry.

Integration of the spectral data yields a value for the OASPL, which are indicated for each respective curve in Fig. 4. Plotting these values with respect to their angular location from the jet centerline shows the directivity of the radiated sound for each nozzle case. Figure 5 illustrates this by comparing the OASPLs of the round and rectangular nozzles. This plot reiterates the fact that, for polar angles between 30–45 deg, the rectangular nozzle's minor plane is louder than the round nozzle by approximately 3 dB, and for greater angles, both rectangular planes are slightly quieter than the round geometry.

The higher noise levels in the minor axis plane (the "noisy plane") are consistent within this study and with numerous previous studies; for example, measurements in a larger aspect ratio rectangular nozzle reported by Kantola [9] and the elliptic jet aeroacoustic study reported by Kinzie and McLaughlin [14]. Their study showed that the flapping mode of elliptic (nonaxisymmetric) jets produces a significant additional noise component in comparison with the major axis ("quiet plane") data. Relating such results to the flyover of a high-performance aircraft, more noise will be produced in the direction of the community directly beneath the aircraft in level flight. The noise radiating to the sidelines will depend on the banking angle of the aircraft.

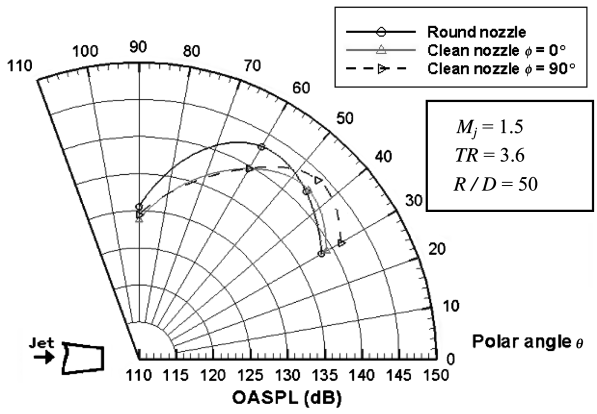

Fig. 5 Directivity comparison for round and rectangular nozzles: $M_j = 1.5$, $U_j/D_{\text{round}} = 59.05$ kHz, $U_j/D_{\text{rect}} = 42.48$ kHz.

Effect of Thrust-Vectoring Attachments

Before investigating the acoustic characteristics of a thrust vectored jet, consideration was given to the influence on the propagated noise attributable to the model's thrust vector attachments

alone. Conducting this "tare" measurement enables the effects of thrust vectoring to then be isolated. Figure 6 compares fully corrected frequency spectra on the major axis of the clean nozzle to that on the major axis of the 0 deg vector nozzle ($\beta = 0$ deg) for a Mach 1.5, heat-simulated jet. Figure 7 presents the same comparison for the minor axis plane. For polar angles 30 and 45 deg from the jet axis, the 0 deg vectored nozzle is slightly quieter than the clean nozzle in the low- to midfrequency range, whereas, in the high-frequency range, there appears to be no difference between the two configurations. These characteristics hold on the minor axis plane as well for polar angles of 60–90 deg (the sideline). The OASPL values are the same within the uncertainty of the measurements, though perhaps slightly higher at the 60 deg polar angle for the 0 deg vectored nozzle on the minor axis plane.

The OASPLs for the major and minor axes results are summarized in Fig. 8 for comparison of each jet's respective noise directivity. Figure 8a represents the major axis plane as indicated by a top view of the vectored nozzle at the plot's origin. Similarly, the minor axis results in Fig. 8b are indicated by the cross section view of the nozzle. (Note that the nozzle sketches are not to scale.) Included in both parts of the figure are data for the round nozzle for additional comparison. It is seen that adding the vectoring attachments reduces the sound levels radiated on the rectangular nozzle's minor axis plane below those of the round nozzle. With respect to the clean nozzle data, the vectoring attachments eliminate the disadvantage of the rectangular nozzle's minor plane being louder than the round geometry for polar angles up to 45 deg. Considered together, the comparisons in Figs. 6–8 show that the general effect of thrust-vectoring attachments (for zero angle deflection) is to lower the sound intensity an average 1 and 2 dB on the major and minor axes, respectively. Finally, it is noteworthy that the shapes of the thrust-vectoring surfaces are much like large chevrons, which have been shown to produce reduced noise levels in round jets being observed in other jet noise experiments [15,16].

Vectored Nozzle Results

Measurements of radiated noise from nozzles simulating thrust vectoring were made for three azimuth angles (the angle of nozzle rotation about its centerline). These orientations are illustrated in Fig. 9 with the respective azimuth angle defined in relation to the polar array of microphones. A test matrix for the thrust-vectoring experiments is provided in Table 2 wherein the nozzle's azimuth angle is identified for each test defined by the jet Mach number M_j and the jet's simulated total temperature ratio relative to the ambient value T_{j0}/Ta. Note that β identifies the angle of vectoring imposed on the flow by the thrust-vectoring attachments. Because there is no difference between azimuth angles 90 and 270 deg for the 0 deg vectored nozzle, only one orientation was necessary to acquire relevant data on the minor axis plane for that case. Similarly, measurements at $\varphi = 180$ deg would also be redundant because of the inherent symmetry of the nozzle.

As mentioned earlier, by injecting helium into the cold jet far enough upstream for thorough mixing with the air, a heated jet (temperature ratio greater than one) is effectively simulated by decreasing the density in the flow and increasing the acoustic Mach Number Uj/a_a [6]. Given that the actual exhaust from turbojet engine aircraft are hot jets, the heat-simulated experiments are justifiably more significant than their cold-jet counterparts, and are thus focused on here. Acoustic spectra were recorded on the rectangular nozzle's minor axis plane with various thrust-vectoring setups and are presented in Fig. 10 for the standard flow conditions of Mach 1.5 and simulated (stagnation) temperature ratio of 3.6.

The data compare results from the 0, 10, and 20 deg vectored nozzles to show the dramatic effect that thrust vectoring has on the acoustic field. This first comparison is made in the quadrant of the minor axis plane (the loudest plane) at an azimuth angle of 90 deg (with the jet deflected toward the microphones). What is seen is that the nonzero vectored nozzles significantly increase the noise across the spectrum at the 90 deg polar angle (Fig. 10d).

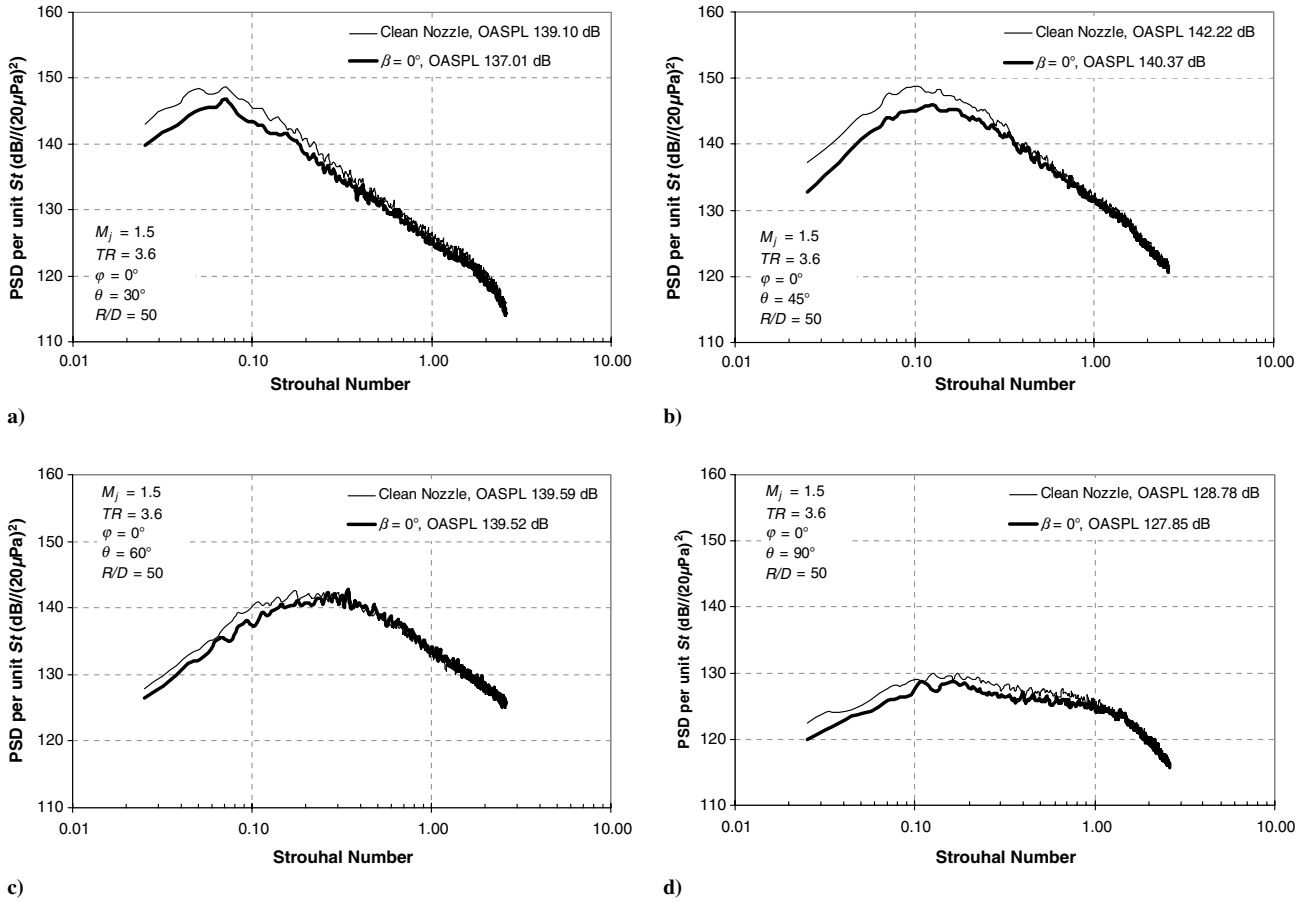

Fig. 6 Comparison of acoustic spectra for clean nozzle with and without vector attachments, major axis plane ($\varphi = 0$ deg): $M_j = 1.5$, $U_j/D = 42.48$ kHz; a) $\theta = 30$ deg, b) $\theta = 45$ deg, c) $\theta = 60$ deg, d) $\theta = 90$ deg.

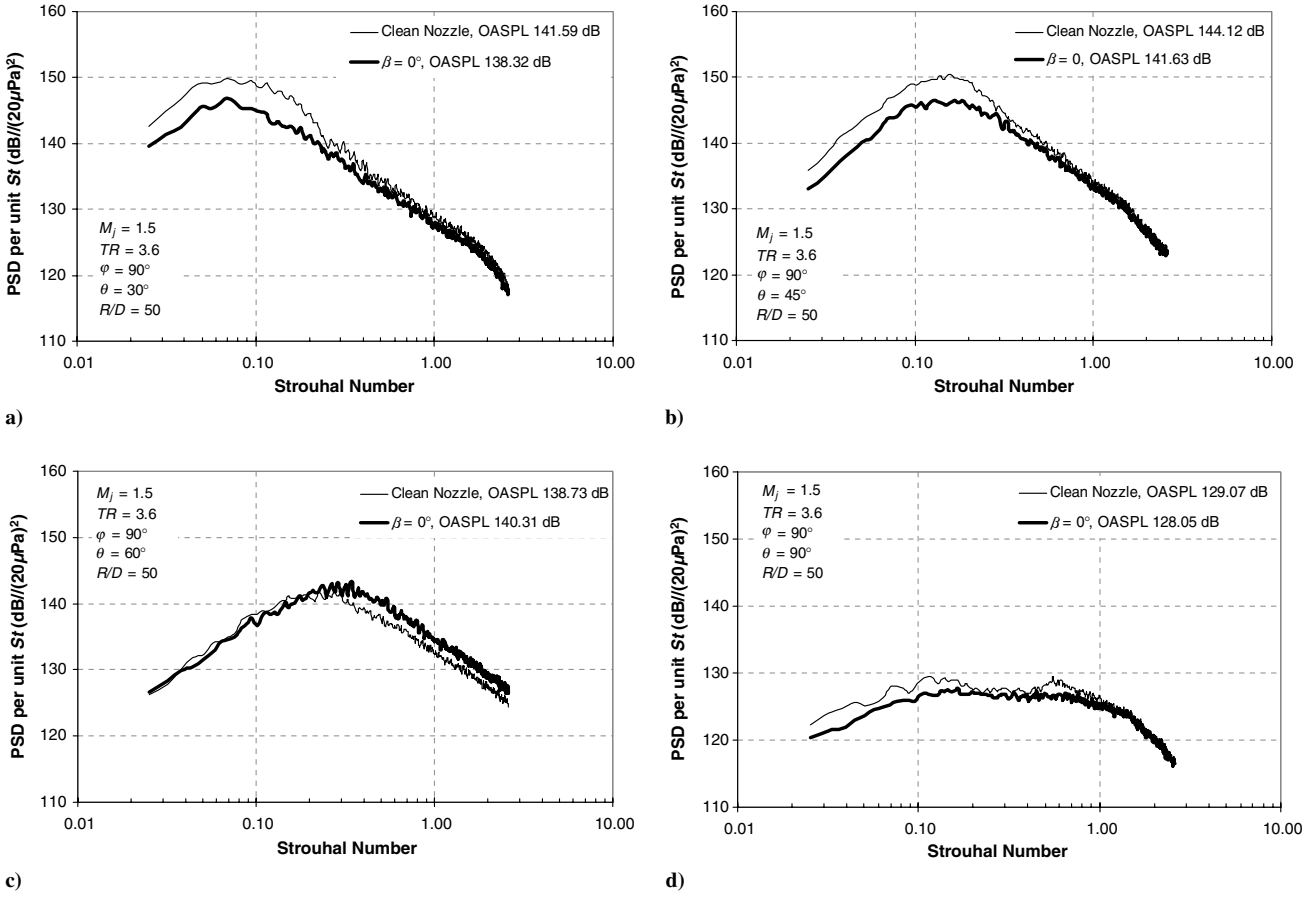

Fig. 7 Comparison of acoustic spectra for clean nozzle with and without vector attachments, minor axis plane ($\varphi = 90$ deg): $M_d = 1.5$, $U_j/D = 42.48$ kHz; a) $\theta = 30$ deg, b) $\theta = 45$ deg, c) $\theta = 60$ deg, d) $\theta = 90$ deg.

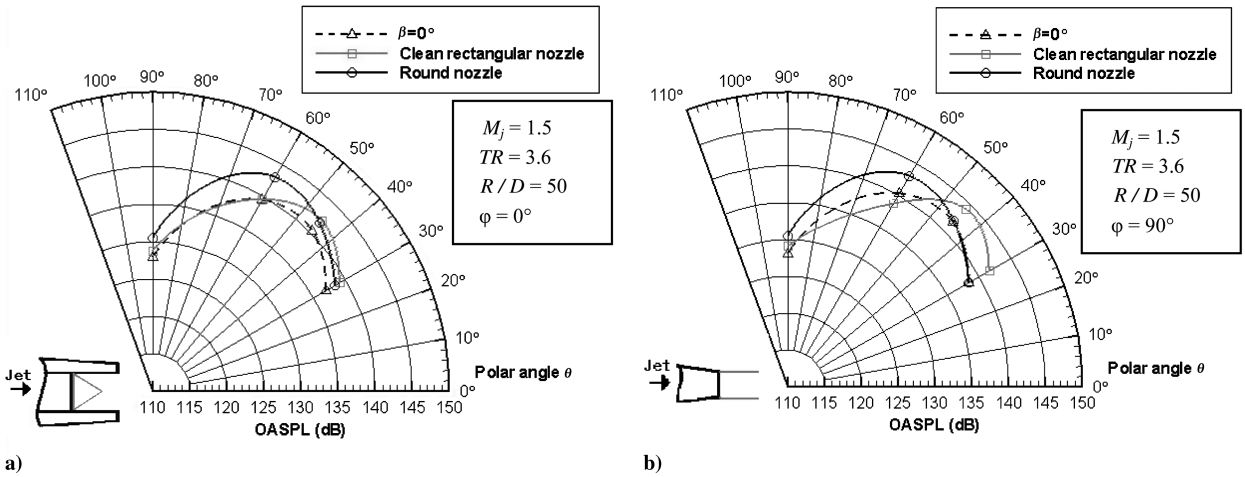

Fig. 8 Directivity comparison for round nozzle and clean nozzle with and without vector attachments: $M_j = 1.5$, $U_j/D_{\text{rect}} = 42.48$ kHz, $U_j/D_{\text{round}} = 59.05$ kHz; a) major axis plane, $\varphi = 0$ deg, b) minor axis plane, $\varphi = 90$ deg.

Table 2 Test conditions for rectangular nozzle experiments including thrust vectoring

Nozzle	M_j	T_{j0}/T_a	U_j/a_a	U_j/D, kHz	Azimuth angles
Clean nozzle (no vectoring paddle)	1.5	3.6	2.37	42.48	0, 90 deg
0 deg thrust vector ($\beta = 0$ deg)	1.5	3.6	2.37	42.48	0, 90 deg
10 deg thrust vector ($\beta = 10$ deg)	1.5	3.6	2.37	42.48	0, 90, 270 deg
20 deg thrust vector ($\beta = 20$ deg)	1.5	3.6	2.37	42.48	0, 90, 270 deg

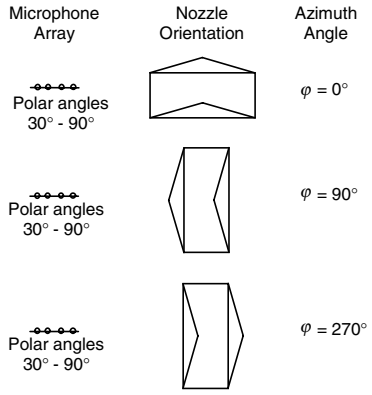

Fig. 9 Vectored nozzle orientations (viewed from downstream).

Additionally, the thrust vectoring effectively reduces the sound pressure level for frequencies in the mid-to-high range for low polar angles (up to 60 deg, Figs. 10a–10c). The decreases occur across a broad range of moderate-to-high frequencies for these polar angles. The energy in the low frequencies emitted from the 10 and 20 deg vectored nozzles is strengthened and exceeds that of the 0 deg vectored nozzle.

To better understand the effect of the thrust-vectoring attachments on the flowfield and the resulting effect on the sound field, schlieren photographs were taken for different vectoring angles, as shown in Fig. 11. Figures 11a and 11b, respectively, show the rectangular nozzle with and without the deflectors. The spreading angles of the jets with the zero angle paddles are slightly larger, and one can observe more small-scale turbulence when the deflectors are present but parallel to the nozzle flow. This is consistent with the general idea of adding a turbulence generator to the lip of the nozzle (such as chevrons or corrugations) to reduce the axial extent of the high-amplitude turbulent structures, and hence the intensity of large-scale mixing noise generated. It thus confirms the reduction of noise observed in the spectra from Fig. 6 to Fig. 8.

The flows depicted in Fig. 11 were all operating with a pressure ratio of 3.67 which produces a Mach 1.5 exit flow corresponding to the design Mach number of the nozzle. Theoretically, the exit flow should be free of shock structures found with pressure imbalanced jet flows. In practice, however, the boundary-layer growth on the nozzle sidewalls (adjacent to the contoured walls) cause secondary flows that prevent the perfectly parallel exit flow.

Figure 11c is a visualization of a rectangular jet with 10 deg flaps and shows an effective deflection of the flow of approximately 8 deg measured to a tolerance of approximately ± 1 deg. To see the effect on the sound directivity, the OASPL was plotted against the polar angle in Fig. 12a. When shifted 8 deg, the OASPL from a nondeflected jet appears to match within 0.5 dB with the OASPL of the 10 deg deflected jet, when the microphones are located in the direction of the deflection ($\varphi = 90$ deg). This shows that the deflection of the flowfield is accompanied by an approximately equal deflection (or rotation) of the sound field. However, the same observation cannot be made on the other side of the jet for $\varphi = 270$ deg, shown in Fig. 12b. This may be due to the triangular shape of the flaps, which are unable to perfectly deflect the entire flow. The part of the flow which is not deflected may produce noise that masks that produced by the deflected part.

Figure 11d is a visualization of a rectangular jet with 20 deg vectoring paddles and shows an effective deflection of the flow of approximately 18 deg. However, when plotting the directivity, shown in Fig. 13, no simple rotation of the sound field matches the rotation of the flowfield. Instead, there seems to be a 4 dB decrease in OASPL at the peak emission, a rotation of the sound field of roughly 10 deg, and an increase of the OASPL at higher polar angles.

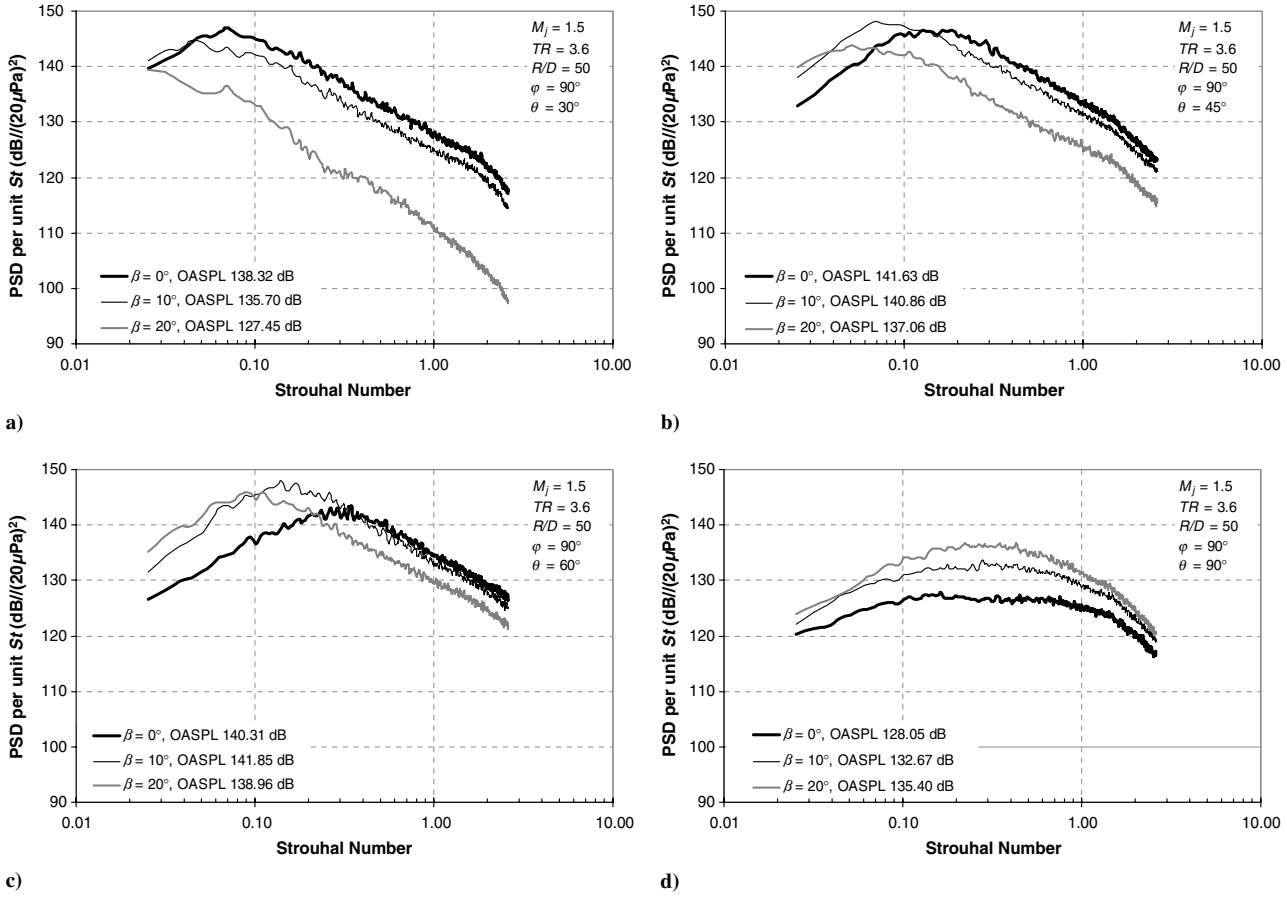

Fig. 10 Comparison of acoustic spectra on the minor axis plane for vectored and nonvectored nozzles: $M_d = 1.5$, $U_j/D = 42.48$ kHz; a) $\theta = 30$ deg, b) $\theta = 45$ deg, c) $\theta = 60$ deg, d) $\theta = 90$ deg.

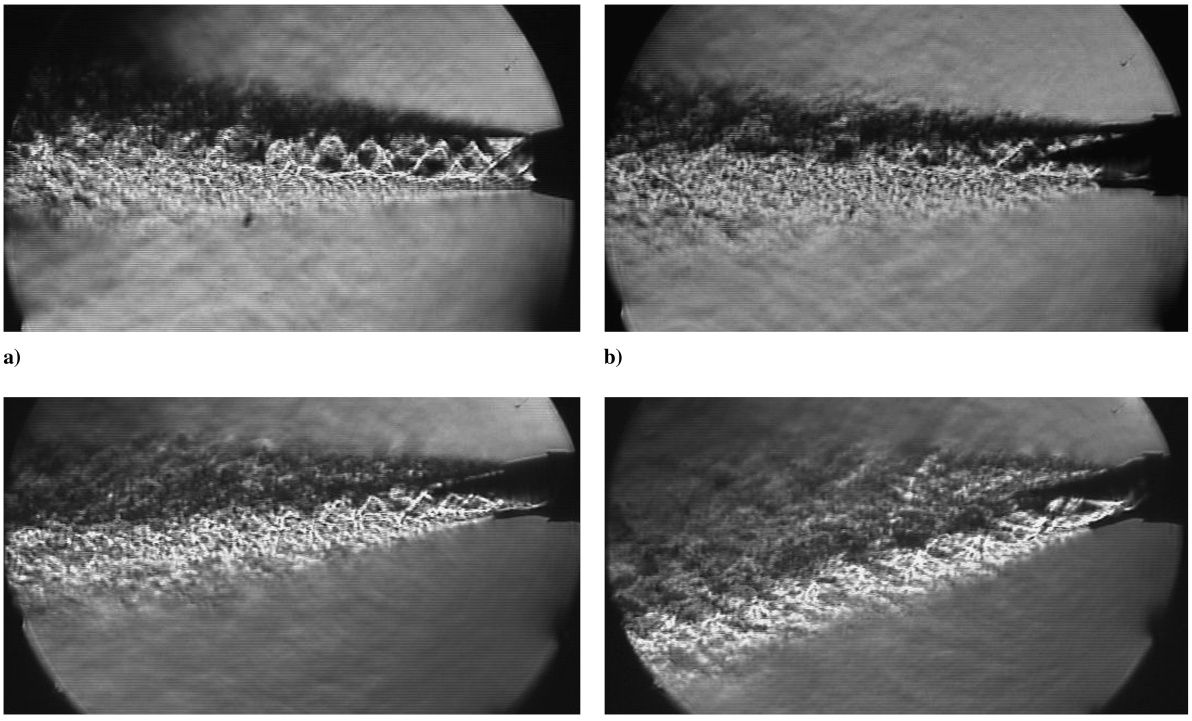

a) b)

c) d)

Fig. 11 Schlieren photographs of a rectangular nozzle, $M_j = 1.5$, $U_j/D = 42.48$ kHz: a) no deflector b) deflector, no vectoring, c) 10 deg vectoring, d) 20 deg vectoring.

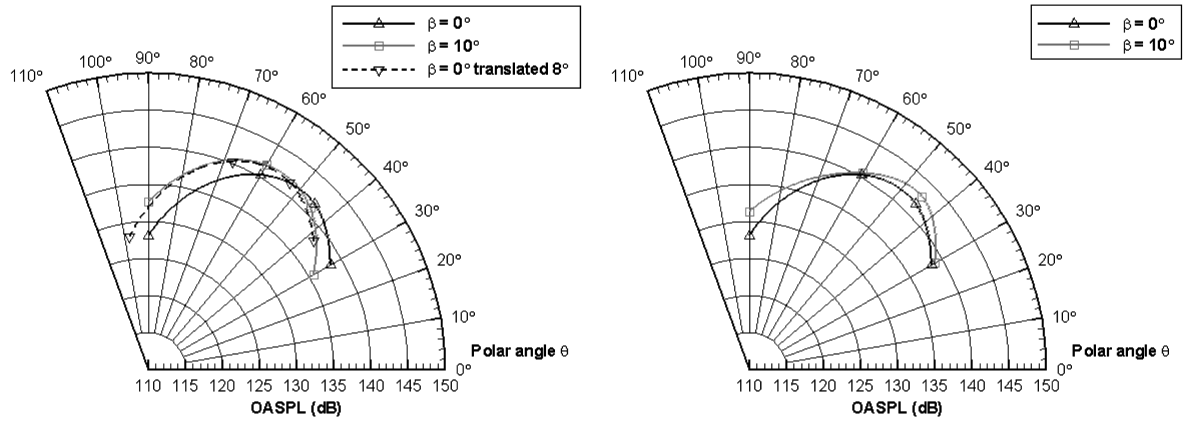

a) b)

Fig. 12 Directivity comparison for a 10 deg deflected jet at $M_j = 1.5$, $T_{j0}/Ta = 3.6$: a) $\varphi = 90$ deg, b) $\varphi = 270$ deg.

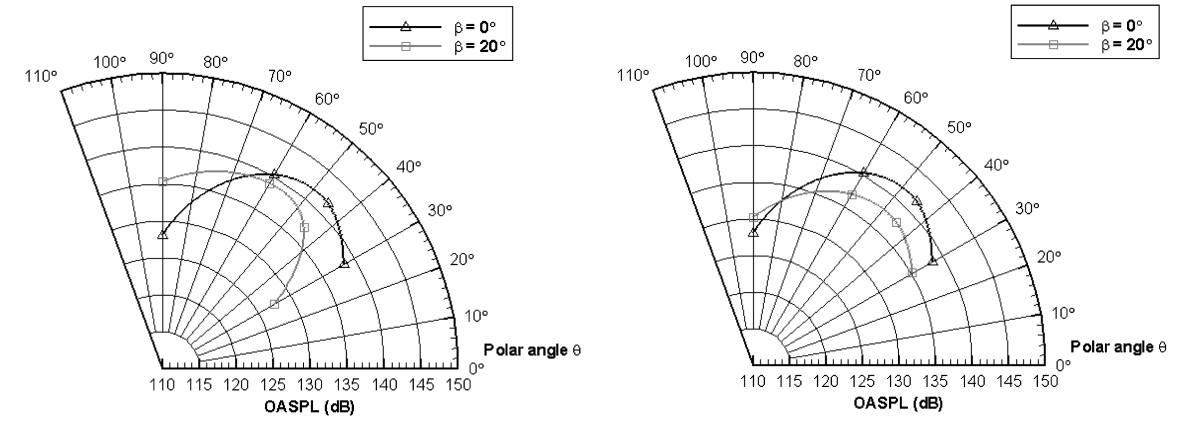

a) b)

Fig. 13 Directivity comparison for a 20 deg deflected jet at $M_j = 1.5$, $T_{j0}/Ta = 3.6$: a) $\varphi = 90$ deg, b) $\varphi = 270$ deg.

It can partly be explained by examining the interaction of the supersonic flow with the compression corner. For a Mach number of 1.5, there is a maximum angle of attack of roughly 12 deg for an attached shock wave to exist. But for higher angles, such as with the 20 deg deflectors, a detached shock is present. Because of the actual shape of the nozzle and deflectors, it is difficult to predict the shock interactions and the resulting decrease in flow velocity. However, the effective Mach number is certainly lower than 1.5, which explains the reduction in OASPL. The enhanced mixing of the deflected flow also explains the higher OASPL at high polar angles, where the broad-scale turbulence mixing noise dominates the radiated noise. Similar observations can be made on the other side of the jet, for $\varphi = 270$ deg, where the OASPL is also observed to be higher at high polar angles. However, the rotation of the sound field is again masked by the portion of the jet which is not deflected, as previously observed with the 10 deg vectoring paddles.

Conclusions

With respect to this research activity, several initial comparisons were made before investigating the acoustic nature of thrust vectoring, the results of which are summarized next.

1) The focus on the nonaxisymmetric nature of the rectangular geometry, temporarily excluding thrust vectoring, revealed the minor axis plane to be louder than the major axis plane by 1–3 dB at polar angles 30–90 deg from the jet centerline.

2) With respect to the round geometry, the rectangular nozzle displayed increased sound intensity in its minor axis plane at polar angles between 30–45 deg from the jet centerline. Sound radiated on the rectangular nozzle's major axis plane showed comparable intensity with the round nozzle for polar angles up to 45 deg and lower intensity for greater angles.

3) By introducing nozzle attachments for the simulation of 0 deg thrust vectoring, the study revealed a decrease in sound pressure level on both axis planes within the low- to midfrequency range. With this decrease, the overall sound pressure levels on both axes of the rectangular nozzle fell below those of the round nozzle for all polar angles. In the high-frequency range, the vectoring attachments seemed to have negligible effect on the generated noise on both axis planes.

4) Experiments conducted with the deflected rectangular exhaust jet showed, as a first-order effect, a deflection/rotation of the acoustic field with the flowfield. Additionally, whereas the OASPL decreases at small polar angles due to the chevron effect of the paddles, the increase of broad-scale turbulent mixing noise generates higher OASPLs at high polar angles. High deflector angles induce the production of a strong shock, which leads to a decrease in mean flow velocity and subsequently in the amount of noise generated. Similarly, due to the triangular shape of the flaps, only part of the flow is deflected, hence creating a nondeflected flow, which partially masks the rotation of the acoustic field produced by the deflected part of the jet. To confirm those observations and the explanations proposed in this paper, it would be interesting to compare the spectra for different values of β with the same polar angle relative to the deflected jet.

Acknowledgments

The authors would like to acknowledge the financial support of the Strategic Environmental Research and Development Program through a subcontract with Wyle Laboratories. The technical monitor for this work was Kenneth Plotkin. Thanks are also expressed to Benoit Petitjean for assistance in the laboratory.

References

[1] Panda, J., "Aeroacoustics," *Aerospace America*, Vol. 43, No. 5, Dec. 2005, p. 12.

[2] Tam, C. K. W., Golebiowski, M., and Seiner, J. M., "On the Two Components of Turbulent Mixing Noise from Supersonic Jets," AIAA Paper 96-1716, 1996.

[3] Tam, C. K. W., Viswanathan, K., Ahuja, K. K., and Panda, J., "The Sources of Jet Noise: Experimental Evidence," *Journal of Fluid Mechanics*, Vol. 615, Nov. 2008, pp. 253–292. doi:10.1017/S0022112008003704

[4] Tanna, H. K., Dean, P. D., and Fisher, M. J., "The Influence of Temperature on Shock-Free Supersonic Jet Noise," *Journal of Sound and Vibration*, Vol. 39, No. 4, 1975, pp. 429–460. doi:10.1016/S0022-460X(75)80026-5

[5] Morris, P. J., Long, L. N., Scheidegger, T. E., and Boluriaan, "Simulations of Supersonic Jet Noise," *Jet Aeroacoustics*, edited by G. Raman, Multi-Science, Essex, England, U.K., 2008.

[6] Doty, M. J., and McLaughlin, D. K., "Acoustic and Mean Flow Measurements of High-Speed, Helium/Air Mixture Jets," *International Journal of Aeroacoustics*, Vol. 2, No. 3, 2003, pp. 293–334. doi:10.1260/147547203322986151

[7] Seiner, J. M., and Ponton, M. K., "Supersonic Acoustic Source Mechanisms for Free Jets of Various Geometries," *Proceedings of teh 78th B Specialists, Meeting On Combat Aircraft Noise*, AGARD, Specialists Printing Services, Essex, England, U.K., Oct. 1991.

[8] Massey, K. C., Ahuja, K. K., and Gaeta, R., "Noise Scaling for Unheated Low Aspect Ratio Rectangular Jets," AIAA Paper 2004-2946, 2004.

[9] Kantola, R. A., "Noise Characteristics of Heated High Velocity Rectangular Jets," *Journal of Sound and Vibration*, Vol. 64, No. 2, 1979, pp. 277–294. doi:10.1016/0022-460X(79)90652-7

[10] Papamoschou, D., "Acoustic Simulation of Hot Coaxial Jets Using Cold Helium-Air Mixture Jets," AIAA Paper 2005-208, 2005.

[11] Petitjean, B. P., and McLaughlin, D. K., "Experiments on the Nonlinear Propagation of Noise from Supersonic Jets," AIAA Paper 2003-3127, May 2003.

[12] Liepmann, H. W., and Roshko, A., *Elements of Gas Dynamics*, Wiley, New York, 1957.

[13] Holder, D. W, and North, R. J., *Schlieren Methods*, National Physical Lab. Notes on Applied Science No. 31, Her Majesty's Stationery Office, London, 1963.

[14] Kinzie, K., and McLaughlin, D. K., "Azimuthal Mode Measurements of Elliptic Jets," *Physics of Fluids*, Vol. 9, No. 7, 1997, pp. 2000–2008. doi:10.1063/1.869319

[15] Rask, O., Gutmark, E., and Martens, S., "The Effect of Chevrons on Broadband Shock Associated Noise," AIAA Paper 2006-0009, Jan. 2006.

[16] Bridges, J., and Brown, C. A., "Parametric Testing of Chevrons on Single Flow Hot Jets," AIAA Paper 2004-2824, 2004.